Journal of
Materials Chemistry A

Materials for energy and sustainability

Accepted Manuscript

This is an Accepted Manuscript, which has been through the Royal Society of Chemistry peer review process and has been accepted for publication.

Accepted Manuscripts are published online shortly after acceptance, before technical editing, formatting and proof reading. Using this free service, authors can make their results available to the community, in citable form, before we publish the edited article. We will replace this Accepted Manuscript with the edited and formatted Advance Article as soon as it is available.

You can find more information about Accepted Manuscripts in the Information for Authors.

ROYAL SOCIETY OF CHEMISTRY

rsc.li/materials-a

Microwave One-pot Synthesis of CNTs-Supported Amorphous Ni-P Alloy Nanoparticles with Enhanced Hydrogenation Performance

Yunqing Kang,[1,2,3] Haoran Du,[1] Bo Jiang,*[1] Hui Li,[1] Yanna Guo,[4] Mohammed A. Amin,[5] Yoshiyuki Sugahara,[2,4] Toru Asahi,[2,4] Hexing Li*[1] and Yusuke Yamauchi*[3,4,6]

1 The Education Ministry Key Lab of Resource Chemistry, Joint International Research aboratory of Resource Chemistry and Shanghai Frontiers Science Center of Biomimetic Catalysis, College of Chemistry and Materials Science, Shanghai Normal University, Shanghai 200234, China

2 Faculty of Science and Engineering, Waseda University, 3-4-1 Okubo, Shinjuku, Tokyo 169-8555, Japan

3 International Center for Materials Nanoarchitectonics (WPI-MANA), National Institute for Materials Science (NIMS), 1-1 Namiki, Tsukuba, Ibaraki 305-0044, Japan

4 Kagami Memorial Research Institute for Materials Science and Technology, Waseda University, 2-8-26 Nishiwaseda, Shinjuku, Tokyo 169-0051, Japan.

5 Department of Chemistry, College of Science, Taif University, P.O. Box 11099, Taif 21944, Saudi Arabia.

6 Australian Institute for Bioengineering and Nanotechnology (AIBN) and School of Chemical Engineering, The University of Queensland, Brisbane, QLD 4072, Australia

Corresponding author's email address:

jiangbo@shnu.edu.cn; hexing-li@shnu.edu.cn; y.yamauchi@uq.edu.au

Abstract

Supported amorphous alloy catalysts have received wide attention due to their unique structural and electronic properties, high catalytic activity, and thermal stability. In this work, a carbon nanotubes (CNTs)-supported amorphous Ni-P alloy nanoparticles (NPs) catalyst is synthesized using a simple one-pot microwave-assisted approach, referred to as Ni-P/CNTs-MA. The prepared Ni-P/CNTs-MA catalyst displays a smaller Ni-P NPs, higher metal dispersion and stronger metal-support interaction than the reference catalyst prepared by the traditional water bath heating method (Ni-P/CNTs-WB). The resulting Ni-P/CNTs-MA catalyst exhibits enhanced catalytic activity for the hydrogenation of nitroarenes compared to the Ni-P/CNTs-WB catalyst. The Ni-P/CNTs-MA catalyst also exhibits improved thermal stability and catalytic durability, probably due to the strong interaction between Ni-P NPs and CNTs.

Keywords: Amorphous Ni-P alloy, Carbon Nanotubes, Microwave synthesis, Selective hydrogenation

Introduction

Substituted aromatic amines are generally synthesized by the chemical selective hydrogenation of nitroarenes, and are industrially important intermediates for pharmaceuticals, agrochemicals, fine-chemicals, dyes, and polymers.[1] Although noble metals catalysts such as Pt, Pd have excellent hydrogenation performance, their high price and limited reserves restrict large-scale applications.[2] In recent years, earth-abundant metals (*e.g.*, Ni, Co, Fe, etc.) have been successfully explored as promising alternatives to noble metal catalysts for hydrogenation of nitroarenes.[3-5] In particular, the nickel phosphide-based catalysts with the advantages of low costs and unique electronic structures exhibit high hydrogen activation and selective hydrogenation of the nitro group.[6] Compared to crystalline nickel phosphide, amorphous Ni-P alloy catalysts have attracted much attention due to their unique structural homogeneity, adjustable composition, and high concentration of coordinatively unsaturated sites.[7] For example, Yang *et al.* [8] reported ordered mesoporous amorphous Ni-P nanowire arrays which had a much higher intrinsic activity for hydrogenation of sugars than the crystalline counterpart due to the amorphous alloy properties and mesoporous material characteristics. However, the poor thermal stability and tendency to agglomerate of amorphous Ni-P alloy nanoparticles (NPs) limit practical applications.

Supported amorphous Ni-P-based catalysts play an important role in heterogeneous catalysis because the large surface area of the support such as silica,[9] carbon nanotubes/graphene,[10,11] and nanofibrous polymer [12] increases the dispersion of metal NPs. In addition, the strong interactions between metal and support can improve the selectivity, activity and durability of the heterogeneous catalysts.[13] However, the preparation of supported amorphous Ni-P alloy catalysts, by traditional synthesis methods, including impregnation-reduction[14] and electrodeposition,[15] generally involves a multi-step preparation process (*e.g.*, impregnation, calcination and reduction of the metal ions).[16] Recently, a microwave-assisted heating method has become a popular strategy in synthetic chemistry.[17] The advantages of microwave irradiation are due to the selective energy absorption of materials and unique thermal effects.[18] This is because microwave heating generates high frequency rotation of polar molecules, producing a quicker and higher heating of species. These species can further form "super hot" dots on the microwave-absorbing materials.[18,19] For example, our group successfully synthesized carbon nanotubes (CNTs) threaded (001) facet-exposed TiO_2 by a microwave-ionothermal strategy,[20] in which CNTs were activated as microwave antennas and form local "super hot" dots to promote

the self-assembly of single crystalline TiO_2 with highly active exposed (001) facets. In addition, microwave irradiation was used to produce UIO-66-NH_2 anchored on graphene which is a highly efficient catalyst for photocatalytic reduction of CO_2.[21] These works demonstrate that the microwave heating method is a promising approach for the preparation of the carbon-based materials supported amorphous Ni-P alloy catalyst with strong metal-support interaction.

We have developed a simple one-pot method to prepare CNTs supported amorphous Ni-P NPs (Ni-P/CNTs-MA) by using a microwave-assisted wet-chemical reduction method, which greatly shortens the synthesis time and enhances the interaction between the amorphous Ni-P NPs and CNTs. Under microwave radiation, the "super hot" dots generated on the surface of CNTs can rapidly induce the nucleation of amorphous Ni-P NPs which are strongly anchored on CNTs. The synthesis conditions, including microwave heating temperature, reaction time, and solvents were optimized. The as-obtained Ni-P/CNTs-MA catalyst exhibits excellent activity, thermal-stability and recyclability for the hydrogenation of nitroarenes.

Results and discussion

A schematic diagram illustrates the synthetic procedure for a CNTs supported amorphous Ni-P NPs (Ni-P/CNTs-MA) catalyst based on a wet-chemical reduction process using microwave heating (**Fig. 1a**). Firstly, the CNTs were dispersed in a mixed water-ethanol solvent containing a Ni precursor ($NiCl_2 \cdot 6H_2O$), a reducing agent (NaH_2PO_2) and a dispersant (CH_3COONa). After adjusting the pH to 11 with 30 wt.% NaOH solution, the above suspension was immediately transferred to the microwave reactor. During microwave heating, the CNTs acted as microwave-antennas, strongly absorbing microwaves and generating many "super hot" dots on the surface. These "super hot" dots facilitate the nucleation of Ni-P on the surface of CNTs, leading to initial well-dispersed amorphous Ni-P nano-nuclei. As the reaction proceeded, the initial Ni-P nano-nuclei grow into Ni-P NPs around the local "super hot" dots on the CNTs *via* absorption of microwave energy. Notably, the microwave-assisted method only takes a very short time (10 min) to complete the entire chemical reduction process. The Ni-P/CNTs-MA catalyst was obtained after washing several times with 8.0 M $NH_3 \cdot H_2O$, deionized water and absolute alcohol, then dried in a vacuum oven. As a comparison, we prepared a typical CNTs supported amorphous Ni-P catalyst using the traditional water bath heating method (Ni-P/CNTs-WB) instead of microwave irradiation. Because of the lack of "super hot" dots in the water bath heating system (at 80 °C), the overall reaction time was at least three hours (see Experimental Section for details). This traditional heating form relies on the thermal conductivity of various compounds or materials, which may have uneven heat transfer in reaction systems, resulting in slow and inefficient heating.[22] However with microwave heating, the high polarity groups such as hydroxyl and carboxyl in CNTs usually have the ability to absorb microwave energy and rapidly convert it to internal energy, thereby forming "super hot" dots.[20] The resulting local high temperature on the surface of CNTs promotes the rapid nucleation of Ni-P NPs.

The transmission electron microscopy (TEM) images with different magnifications of the prepared Ni-P/CNTs-MA sample are shown in **Fig. 1b,c**. The Ni-P NPs, with a particle size of ~71 nm, are successfully anchored to the CNTs and exhibit a good dispersion. The diffractive halo-like selected-area electron diffraction (SAED) pattern (**Fig. 1d)** confirms the amorphous feature of Ni-P NPs. In contrast, the Ni-P nanospheres with large particle size (~135 nm) are randomly distributed on the CNTs for Ni-P/CNTs-WB prepared by the water bath heating method (**Fig. S1**). These results indicate that the "super hot" dots produced by microwave irradiation can quickly induce the formation of large number of nucleation, thus generating

much smaller sized Ni-P NPs.

The amorphous structure of Ni-P NPs is further confirmed by wide-angle X-ray diffraction (XRD) (**Fig. 2a**). Bare CNTs show a typical crystalline XRD pattern with obvious diffraction peaks at 26.1, 42.3, 44.3 and 54.5°, corresponding to the (002), (100), (101) and (004) crystal planes of hexagonal graphite (JCPDS 41-1487), respectively.[23] One impurity peak at $2\theta = 37.1°$ is also observed. After loading Ni-P NPs, no diffraction peaks of Ni-P are observed, indicating the amorphous nature of Ni-P in Ni-P/CNTs-MA. A similar result was also observed in Ni-P/CNTs-WB sample (**Fig. S2**). **Fig. 2b** shows N_2 adsorption-desorption isotherms and the pore size distribution curve of bare CNTs and Ni-P/CNTs-MA. The Ni-P/CNTs-MA exhibits similar adsorption-desorption isotherms and pore structure with CNTs, revealing that Ni-P NPs loading does not change the support structure. The surface areas of Ni-P/CNTs-WB and Ni-P/CNTs-MA are 126.9 m^2g^{-1} and 124.1 m^2g^{-1}, respectively, which are smaller than that of pure CNTs (131.2 m^2g^{-1}) (**Table 1**). The pore volume of Ni-P/CNTs-WB and Ni-P/CNTs-MA also show a slight decrease compared to bare CNTs, which is likely due to that the amorphous Ni-P NPs that cover the surface and pores of CNTs.

The compositions of the samples were confirmed by inductively coupled plasma optical emission spectroscopy (ICP), (**Table 1)**. The results show that the P content in Ni-P/CNTs-MA sample is slightly higher than that of Ni-P/CNTs-WB, which may be attributed to the faster nucleation speed and easier combination of Ni and P under microwave irradiation. Moreover, the metal dispersion ratio in Ni-P/CNTs-MA measured by H_2-TPD is 21.2 %, which is much higher than that of Ni-P/CNTs-WB (16.1 %), attributed to the fast formation of Ni-P NPs under microwave irradiation.

X-ray photoelectron spectroscopy (XPS) was used to characterize the electronic states on the Ni and P of Ni-P/CNTs-MA catalyst. As shown in **Fig. 2c**, the high-resolution XPS spectrum of Ni 2*p* can be deconvoluted into six peaks. The main peaks at 853.2 eV and 870.5 eV can be attributed to the $2p_{3/2}$ and $2p_{1/2}$ peak of metallic Ni^0 in Ni-P/CNTs-MA, respectively, whereas the peaks located at 856.2 and 874.3 eV correspond to $2p_{3/2}$ and $2p_{1/2}$ from nickel oxides (NiO_x) species. Two satellite peaks at 861.4 and 879.8 eV could also be observed, indicating spontaneous surface oxidation upon exposure to air.[23] For the P 2*p* spectrum (**Fig. 2d**), peaks located at 130.7 eV ($2p_{1/2}$) and 129.1 eV ($2p_{3/2}$) can be assigned to P^0 (P-metal), with the peak at 133.4 eV indexed to the oxidized P species.[24] Notably, the binding energy (BE) of Ni $2p_{3/2}$ (853.2 eV) is positively shifted compared to the reported metal Ni (852.6 eV),[24] whereas the BE of P $2p_{3/2}$ (129.1 eV) is negatively shifted

relative to the reported elemental P (130.2 eV).[26] These results indicate that the charge transfer from Ni to P in the Ni-P/CNTs-MA catalyst. A similar electron-donating phenomenon of metallic Ni can be observed in Ni-P/CNTs-WB catalyst (**Fig. S3**). Compared to Ni-P/CNTs-WB, the Ni 2*p* in Ni-P/CNTs-MA catalyst slightly shifts toward a higher binding energy, which may be due to the higher content of P (**Table 1**) in Ni-P/CNTs-MA sample.[27] Previous studies have also demonstrated that charge transfer between metal and P can improve the selectivity and activity of M-P catalyst for hydrogenation reactions.[12,28]

Fourier transform infrared (FTIR) and Raman spectra of as-prepared catalysts and bare CNTs are shown in **Fig. 2e,f**. The peaks at 1190, 1575, 1722 and 3430 cm^{-1} are ascribed to the C–C stretching, aromatic ring stretching, C=O stretching and H–O stretching, respectively.[29] After loading amorphous Ni-P NPs, no significant changes in the FTIR is observed in the Ni-P/CNTs-WB and Ni-P/CNTs-MA samples (**Fig. 2e**). Raman spectroscopy is an effective technique to understand the incorporation of heteroatoms in carbon materials.[30,31] As shown in **Fig. 2f**, the typical Raman bonds of CNTs at 1324.8 cm^{-1} and 1574.5 cm^{-1} are observed, which corresponding to the *D* and *G* bands, respectively. The intensity ratio (I_D/I_G) of the *D* and *G* band is usually used to describe the surface defects and disorders of carbon materials.[32,33] The I_D/I_G of Ni-P/CNTs-MA (1.42) is higher than Ni-P/CNTs-WB (1.35) and CNTs (1.26), suggesting that microwave-assist heating method increases the numbers of defect sites. The increased defects in CNTs could enhance charge transformation and the adsorption of reactants which increases the catalytic activity, as reported by Yang and co-workers.[34]

H_2-TPD and EIS spectra of the Ni-P/CNTs-MA and Ni-P/CNTs-WB catalysts are shown in **Fig. S4**. The broad hydrogen desorption peak at high temperatures (between 300 °C and 500 °C) can be attributed to the hydrogen-storage ability of CNTs in both Ni-P/CNTs-MA and Ni-P/CNTs-WB samples (**Fig. S4a**).[35] The desorption peak at moderate temperature (less than 300 °C) represents the adsorption of hydrogen by amorphous Ni-P NPs. From the H_2-TPD data, it is revealed that the Ni-P/CNTs-MA catalyst exhibits a lower desorption temperature than the Ni-P/CNTs-WB catalyst. This result indicates Ni-P/CNTs-MA has a weaker absorption bond between the hydrogen atoms and the active sites compared with Ni-P/CNTs-WB, which may facilitate the transfer of the adsorbed hydrogen atoms to the adsorbed reactants to promote hydrogenation reactions.[14] The electrochemical impedance spectroscopy (EIS) measurements in **Fig. S4b** show that the Ni-P/CNTs-MA catalyst has a smaller semicircle than Ni-P/CNTs-WB catalyst in the low-frequency range,

suggesting a lower charge transfer resistance (R_{ct}).[36] The strong metal-support interaction and highly metal dispersion in Ni-P/CNTs-MA catalyst is more conducive to lower R_{ct} value and faster charge transfer efficiency.

Transition metal phosphides have shown outstanding catalytic performance in many applications including hydrogen evolution reaction (HER),[37] oxygen evolution reaction (OER),[38] CO_2 conversion,[39,40] and hydrogenation reactions.[28] In particular, the amorphous Ni-P alloy catalysts have high activity in a wide range of hydrogenation reactions, probably due to the highly unsaturated metal active sites in amorphous structure and the electronic interaction between Ni and P.[7] In this work, we used the selective hydrogenation of nitroarenes to primary amines as the probe reaction to study the catalytic performance of Ni-P/CNTs-MA.

The catalytic performance was measured by the selective hydrogenation of *p*-chloronitrobenzene (*p*-CNB) to *p*-chloroaniline (*p*-CAN). To explore the influence of the preparation process on catalyst activity, we optimized the microwave reaction conditions, including reaction temperature/time, heating rate and solvents (**Fig. S5**) for preparation of catalysts. As seen in **Fig. S5a-b**, the optimal microwave preparation temperature is 80 °C with a heating time of 10 min. Then, the optimal time at 80 °C (**Fig. S5c**) and the mixed solvent ratio (water + ethanol) (**Fig. S5d**) were also optimized. In general, the energy dissipation factor (tan δ) reflects the efficiency with which molecules convert microwave radiation into heat energy.[41] The larger value of ethanol (EtOH) (tan $\delta = 0.94$) than water (tan $\delta = 0.13$) indicates that EtOH is more effective at absorbing microwaves[42] so that ethanol may extremely affect the absorption of microwave by CNTs, which is not beneficial to quickly generate "super hot" dots on CNTs. However, small amount of ethanol is not appropriate for the dispersion of CNTs in mixed solvents. Finally, the optimum ratio of water:ethanol for the catalyst microwave preparation was found to be 40:10 (**Fig. S5d**).

In addition to the above adjustment of the catalyst microwave preparation conditions, we also optimized the hydrogenation reaction conditions. The reaction conditions, including reaction time, temperature and hydrogen pressure for Ni-P/CNTs-MA catalyst were outlined in **Fig. 3**. With the increase in reaction time (**Fig. 3a**), the best *p*-CAN yield (97.5%) is obtained at 100 minutes. As **Fig. 3b** shown, the activity of hydrogenation of *p*-CNB is proportional to the reaction pressure and reach the highest activity at 3 MPa. It is well known that the reaction rate increases with the increase in temperature. However, if the temperature reaches 120 °C, the *p*-CNB yield decreases from 97.5% (at 110 °C) to 96.4 %, which may because of the

dechlorination of some *p*-CAN (**Fig. 3c**). Therefore, the final reaction conditions were 110 °C, 3 MPa and 100 minutes. The negligible hydrogenation activity of bare CNTs indicates that Ni-P NPs are the active sites for *p*-CNB hydrogenation. Significantly, the yield of *p*-CAN in Ni-P/CNTs-MA catalyst is almost three times higher than Ni-P/CNTs-WB catalyst under the same reaction conditions (**Fig. 3d**).

Stability is an important criterion for catalyst performance. Therefore, the thermal stability and recycle stability of Ni-P/CNTs-MA and Ni-P/CNTs-WB were investigated. **Fig. 4a** shows the XRD patterns of the Ni-P/CNTs-MA and the thermal treated Ni-P/CNTs-MA at 400 °C (Ni-P/CNTs-MA-400) for 2 h in N_2 atmosphere. The crystalline structure of Ni and Ni_3P could be observed in the XRD after thermal treatment, which is in agreement with the TEM image (**Fig. S6a,b**), where the clear lattice spacing of d = 0.2 nm (corresponding to the (111) plane of *fcc* Ni) can be observed at the edges of the Ni-P particle (**Fig. 4b**). A similar crystallization phenomenon (**Fig. S6c,d**) can be observed in the Ni-P/CNTs-WB sample after calcination at 400 °C (Ni-P/CNTs-WB-400). After thermal treatment, the relative activities of Ni-P/CNTs-MA-400 and Ni-P/CNTs-WB-400 for hydrogenation of *p*-CNB decreased by 31% and 62%, respectively, compared to their fresh counterparts (**Fig. 4c**). This indicates that Ni-P/CNTs-MA exhibits a much better thermal stability than Ni-P/CNTs-WB. **Fig. 4d** demonstrates that the recycling stability of Ni-P/CNTs-MA is also better than that of Ni-P/CNTs-WB. The relative hydrogenation activity is 88% for the Ni-P/CNTs-MA after four uses, while the relative activity of Ni-P/CNTs-WB is only 42%. TEM, XRD and XPS measurements (**Fig. S7**) after the recycling hydrogenation test were performed to investigate the morphology, crystal structure and chemical state of the Ni-P/CNTs-MA catalyst. The TEM image in **Fig. S7a** shows that the morphology of Ni-P/CNTs-MA did not change significantly after the stability test. Compared to the fresh catalyst, the Ni-P in Ni-P/CNTs-MA after recycling test still maintains its amorphous feature as revealed by the XRD pattern (**Fig. S7b**). The XPS results (**Fig. S7c**) show that the NiO*x* species of Ni-P/CNTs-MA increase on the surface compared with fresh one after the stability test.

In order to demonstrate that the catalyst has a universality for hydrogenation reactions, we used substrates for the hydrogenation of other industrially interesting nitroarenes (**Table 2**). With the same reaction conditions, both Ni-P/CNTs-MA and Ni-P/CNTs-WB show high selectivity for primary amines, but the conversion activity of Ni-P/CNTs-MA is 2.8-3.3 times higher than Ni-P/CNTs-WB catalyst. This indicates that the Ni-P/CNTs-MA catalyst has a remarkable conversion activity for the hydrogenation of nitroarenes to primary

amines.

Conclusion

In summary, we report a new microwave-assisted heating strategy for preparing CNTs supported amorphous Ni-P nanoparticles (Ni-P/CNTs-MA) catalyst for selective hydrogenation of nitroarenes. The Ni-P/CNTs-MA catalyst has much higher activity and thermal/recycle stability than the Ni-P/CNTs-WB sample prepared by traditional water bath heating method. The outstanding hydrogenation performance of Ni-P/CNTs-MA catalyst can be attributed to the high-dispersion of amorphous Ni-P NPs and enhanced interaction between the Ni-P NPs and the CNTs support, due to the "super hot" dots effect induced by microwave irradiation. It is expected that this microwave-assisted reduction method could be extended to other metal alloys (*e.g.,* Ni(CoFe)-P, Ni(CoFe)-B-P) anchored on various supports (*e.g.,* graphene, MXene), for use in other fields such as CO_2 conversion and electrocatalytic water splitting.

Experimental Section

Materials. All chemicals and solvents were of analytical grade and were used as received without further purification. Nickel(II) chloride hexahydrate ($NiCl_2 \cdot 6H_2O$, >98.0%) were obtained from Sinopharm Chemical Reagent Co., Ltd. (Shanghai, China). Sodium hypophosphite (NaH_2PO_2, 99.0%) was bought from Macklin Ltd. (Shanghai, China). Sodium acetate (CH_3COONa, 99%) was obtained from Adamas Reagent Co., Ltd. Carbon nanotubes (CNTs, >90%) were brought from Aladdin Ltd. (Shanghai, China). NaOH, $NH_3 \cdot H_2O$ and all solvent were purchased from Sinopharm Chemical Reagent Co., Ltd. (Shanghai, China).

Catalyst preparation. The microwave-assist synthesis of CNTs supported amorphous Ni-P alloy (Ni-P/CNTs-MA) catalyst was prepared by the following procedures: 1.9 g CNTs, 0.41 g $NiCl_2 \cdot 6H_2O$, 0.76 g NaH_2PO_2 and 0.14 g CH_3COONa was dissolved in 50 mL mixed solvent of deionized water and ethanol with a volume ratio of 40:10. Next, the mixture was stirred at 38 °C for 2 h and then the pH was adjusted to 11 by 30 wt.% NaOH aqueous solution. After stirring for another 30 min, the solution was transferred to a microwave oven (Ethos TC. Milestone) for reaction with a specific heating rate. The effect of *p*-CNB hydrogenation activity of Ni-P/CNTs-MA on different microwave preparation conditions was carefully investigated, as shown in **Fig. S5**. Then, we found the optimal microwave preparation conditions to prepare the catalyst. After heating, the

catalyst was washed several times with 8 M $NH_3 \cdot H_2O$, deionized water and absolute alcohol and finally dried under vacuum at 50 °C overnight for further use. For comparison, a reference CNTs-supported amorphous Ni-P alloy (Ni-P/CNTs-WB) catalyst was also prepared using the same procedure with water bath heating instead of microwave irradiation. Typically, the mixed solution after adjusting the pH to 11 was heated up to 80 °C in a closed water bath and stirred for at least three hours. The obtained black product was washed several times with 8 M $NH_3 \cdot H_2O$, deionized water and absolute alcohol, and finally dried under vacuum at 50 °C overnight before use.

Characterization. The structure of catalysts was determined by both X-ray diffraction (XRD; Rigaku D/Max-RB with Cu Kα radiation) and Selected area electronic diffraction (SAED; JEOL JEM-2100). Transmission electron microscopy (TEM, JEOL-2010F) were employed to observe morphology and the particle size. The N_2 adsorption-desorption isotherms were measured at 77 K using a Micromeritics ASAP 2010 instrument. The pore size distribution curves were obtained by the Barrett-Joyner-Halenda (BJH) method. The surface electronic states were investigated by X-ray photoelectron spectroscopy (XPS; ULVAC-PHI PHI5000 Versa Probe using Al Kα radiation), during which all catalyst samples were dried and pretreated in situ in a pure Ar atmosphere to avoid oxidation. The hydrogen temperature-programmed desorption (H_2-TPD) was tested using a Micromeritics-2920. The bulk composition was analyzed by means of inductively coupled plasma optical emission (ICP; Varian VISTA-MPX). Electrochemical impedance spectroscopy (EIS) was carried out in a standard three-electrode using an electrochemical station (CHI660E). The working electrode was the catalyst loaded on conductive glass (FTO glass) with a working area of 2.25 cm^2. The counter electrode and the reference electrode were platinum sheet and saturated calomel electrode (SCE), respectively. The bias voltage was 0.3 V and a Na_2SO_4 (0.5 M) aqueous solution was used as the electrolyte. The results were recorded over a frequency ranging from 0.1 to 10^5 Hz.

Hydrogenation activity test. Typically, the hydrogenation reaction was performed in a 100 mL high-pressure stainless-steel autoclave, in which the catalyst (containing 0.14 mmol Ni) was mixed with 7.0 mmol substrate, 0.5 mL 1,3,5-trimethylbenzene (internal standard) and 20 mL EtOH. After replacing all the air with H_2 in the autoclave three times, the reactor was filled with H_2 up to 3 MPa. Then it was heated to 110 ˚C at a stirring rate of 1,050 rpm, which was sufficient to eliminate the diffusion limit. After the reaction, the final products were monitored by GC (Agilent 7890B equipped with a DB-624 30 m×0.320 mm capillary column).

Conflicts of interest

There are no conflicts of interest to declare.

Author contributions

Yunqing Kang: Investigation, Visualization, Formal analysis, Writing-original draft. Haoran Du: Investigation, Formal analysis. Bo Jiang: Investigation, Formal analysis, Writing-Review & Editing. Hui Li: Conceptualization, Formal analysis. Yanna Guo: Investigation, Formal analysis. Mohammed A. Amin: Investigation, Formal analysis. Yoshiyuki Sugahara: Investigation, Formal analysis. Toru Asahi: Supervision, Investigation. Hexing Li: Supervision, Resources, Writing-Review & Editing, Project administration. Yusuke Yamauchi: Supervision, Validation, Visualization, Project administration.

Acknowledgements

This work was supported by the National Natural Science Foundation of China (21761142011), a Research Grant from the Chinese Ministry of Science and Technology (2020YFA0211004), the Shanghai Local Government (21ZR1446600), the “111” Innovation and Talent Recruitment Base (D18020), and the JST-ERATO Yamauchi Materials Space-tectonics (JPMJER2003). The authors are also grateful to the Taif University Researchers Supporting Project number (TURSP-2020/03), Taif University, Taif, KSA. The authors also acknowledge financial support from the China Scholarship Council (CSC). This work was performed in part at the Queensland node of the Australian National Fabrication Facility, a company established under the National Collaborative Research Infrastructure Strategy to provide nano and microfabrication facilities for Australia’s researchers.

Reference

1 J. Song, Z.-F. Huang, L. Pan, K. Li, X. Zhang, L. Wang, J.-J. Zou, *Appl. Catal. B*, 2018, **227**, 386.

2 H.-U. Blaser, H. Steiner, M. Studer, *ChemCatChem* 2009, **1**, 210.

3 Y. Sun, X. Li, Z. Cai, H. Bai, G. Tang, Z. Hou, *Catal. Sci. Technol.*, 2018, **8**, 4858.

4 Y. Zhu, S. Yang, C. Cao, W. Song, L.-J. Wan, *Inorg. Chem. Front.*, 2018, **5**, 1094.

5 Y. Shi, M. Li, Y. Yu, B. Zhang, *Energy Environ. Sci.*, 2020, **13**, 4564.

6 H. Wang, Y. Shu, M. Zheng, T. Zhang, *Catal. Lett.*, 2008, **124**, 219.

7 Y. Pei, G. Zhou, N. Luan, B. Zong, M. Qiao, F. Tao, *Chem. Soc. Rev.*, 2012, **41**, 8140.

8 Y. Yang, H. Gu, Q. Zhang, H. Li, H. Li, *ACS Appl. Mater. Interfaces*, 2020, **12**, 26101.

9 J.-F. Deng, X. Zhang, E. Min, *Appl. Catal.*, 1988, **37**, 339.

10 W.X. Chen, J.P. Tu, H.Y. Gan, Z.D. Xu, Q.G. Wang, J.Y. Lee, Z.L. Liu, X.B. Zhang, *Surf. Coat. Technol.*, 2002, **160**, 68.

11 X. Du, C. Yang, X. Zeng, T. Wu, Y. Zhou, P. Cai, G. Cheng, W. Luo, *Int. J. Hydrogen Energy*, 2017, **42**, 14181.

12 K. Liu, Y. Wang, P. Chen, W. Zhong, Q. Liu, M. Li, Y. Wang, W. Wang, Z. Lu, D. Wang, *Appl. Catal. B*, 2016, **196**, 223.

13 T.W. van Deelen, C. Hernández Mejía, K.P. de Jong, *Nat. Catal.*, 2019, **2**, 955.

14 H. Li, W. Wang, H. Li, J.-F. Deng, *J. Catal.*, 2000, **194**, 211.

15 G. Xie, Z. Lü, G. Wang, *Mater. Chem. Phys.*, 2009, **118**, 281.

16 S. Anantharaj, S. Noda, *Small*, 2020, **16**, 1905779.

17 A. de la Hoz, Á. Díaz-Ortiz, A. Moreno, *Chem. Soc. Rev.*, 2005, **34**, 164.

18 Y. Li, H. Huang, Y. Xiong, S.V. Kershaw, A.L. Rogach, *Angew. Chem. Int. Ed.*, 2018, **57**, 5833.

19 J. Remón, G. Zhu, V.L. Budarin, J.H. Clark, *Green Chem.*, 2018, **20**, 2624.

20 S. Xiao, W. Zhu, P. Liu, F. Liu, W. Dai, D. Zhang, W. Chen, H. Li, *Nanoscale*, 2016, **8**, 2899.

21 X. Wang, X. Zhao, D. Zhang, G. Li, H. Li, *Appl. Catal. B*, 2018, **228**, 47.

22 M. Baghbanzadeh, L. Carbone, P. D. Cozzoli, C. O. Kappe, *Angew. Chem. Int. Ed.*, 2011, **50**, 11312.

23 M. Shao, D. Wang, G. Yu, B. Hu, W. Yu, Y. Qian, *Carbon*, 2004, **42**, 183.

24 M. C. Biesinger, B. P. Payne, A. P. Grosvenor, L. W.M. Lau, A. R. Gerson, R. S.C. Smart, *Appl. Surf. Sci.*, 2011, **257**, 2717.

25 T.I. Korányi, *Appl. Catal. A*, 2003, **239**, 253.

26 Y. Pan, Y. Liu, J. Zhao, K. Yang, J. Liang, D. Liu, W. Hu, D. Liu, Y. Liu, C. Liu, *J. Mater. Chem. A*,

2015, **3**, 1656.

27 Q. Liu, C. Tang, S. Lu, Z. Zou, S. Gu, Y. Zhang, C. M. Li, *Chem. Commun.* 2018, **54**, 12408.

28 R. Gao, L. Pan, H. Wang, X. Zhang, L. Wang, J.-J. Zou, *ACS Catal.*, 2018, **8**, 8420.

29 J. Chen, Z. H. Zhu, Q. Ma, L. Li, V. Rudolph, G. Q. Lu, *Catal. Today*, 2009, **148**, 97.

30 Y.-g. Wu, M. Wen, Q.-S. Wu, H. Fang, *J. Phys. Chem. C*, 2014, **118**, 6307.

31 X. Cui, Y. Long, X. Zhou, G. Yu, J. Yang, M. Yuan, J. Ma, Z. Dong, *Green Chem.*, 2018, **20**, 1121.

32 L. Liu, P. Concepción, A. Corma, *J. Catal.*, 2016, **340**, 1.

33 D. Luo, G. Zhang, J. Liu, X. Sun, *J. Phys. Chem. C*, 2011, **115**, 11327.

34 H. Yang, S. Song, R. Rao, X. Wang, Q. Yu, A. Zhang, *J. Mater. Chem. A*, 2010, **323**, 33.

35 Y. Ju, F. Li, *J. Nat. Gas Chem.*, 2006, **15**, 313.

36 J. N. Balaraju, V. E. Selvi, V. K. W. Grips, K. S. Rajam, *Electrochim. Acta*, 2006, **52**, 1064.

37 Y. Shi, B. Zhang, *Chem. Soc. Rev.*, 2016, **45**, 1529.

38 Z. Pu, T. Liu, I. S. Amiinu, R. Cheng, P. Wang, C. Zhang, P. Ji, W. Hu, J. Liu, S. Mu, *Adv. Funct. Mater.*, 2020, **30**, 2004009.

39 F. Geng, Y. Bonita, V. Jain, M. Magiera, N. Rai, J. C. Hicks, *Ind. Eng. Chem. Res.*, 2020, **59**, 6931.

40 U. Guharoy, T. Ramirez Reina, S. Gu, Q. Cai, *J. Phys. Chem. C*, 2019, **123**, 22918.

41 M. Tsuji, M. Hashimoto, Y. Nishizawa, M. Kubokawa, T. Tsuji, *Chem.– Eur. J.*, 11(2) (2005) 440-452.

42 D. Dallinger, C. O. Kappe, *Chem. Rev.*, 2007, **107**, 2563.

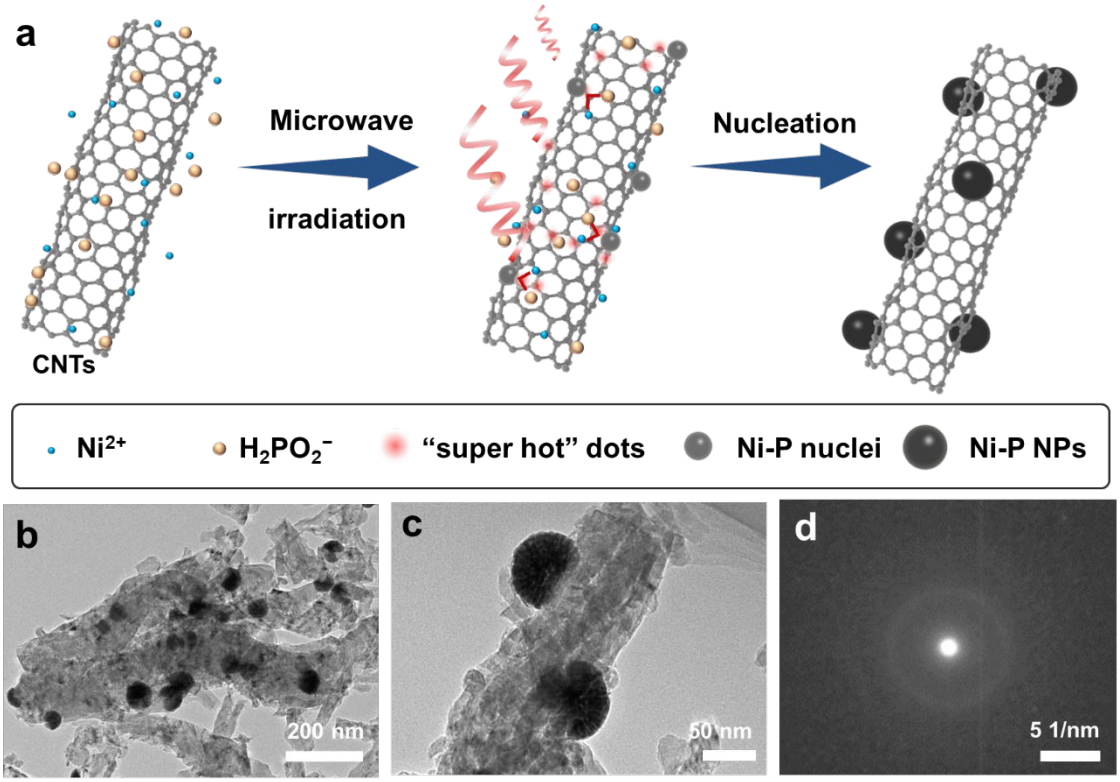

Fig. 1. (a) A schematic illustration of the procedures for preparing Ni-P/CNTs-MA using microwave irradiation. (b) Low- and (c) high- magnification TEM images of the Ni-P/CNTs-MA catalyst. (d) The corresponding SAED pattern of Ni-P NPs.

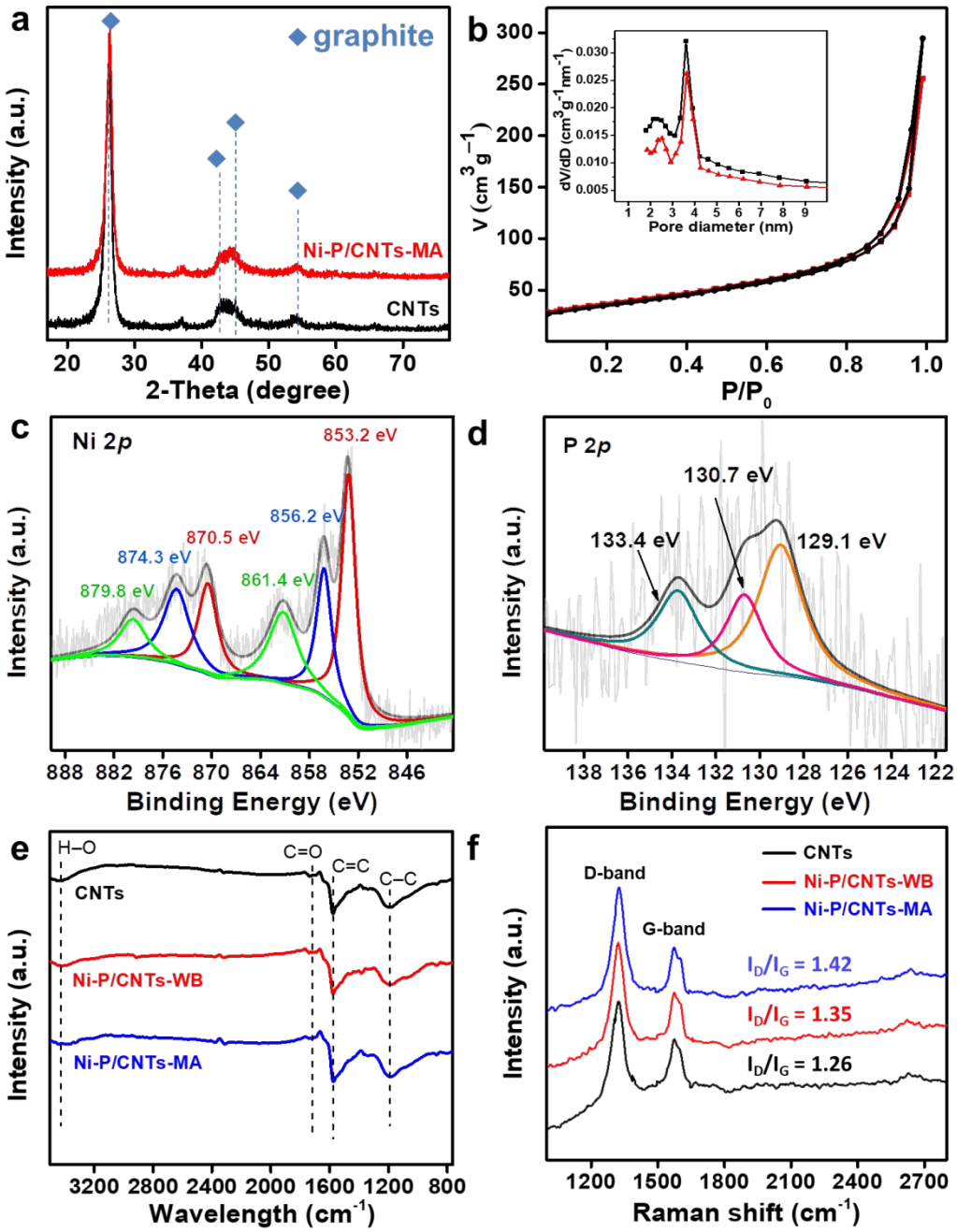

Fig. 2. (a) XRD patterns and (b N_2 adsorption−desorption isotherm of Ni-P/CNTs-MA catalyst and bare CNTs (Inset shows the pore size distribution). XPS spectra of (c) Ni 2*p* and (d) P 2*p* of Ni-P/CNTs-MA catalyst. (e) FT-IR and (f) Raman spectra of Ni-P/CNTs-MA, Ni-P/CNTs-WB and bare CNTs.

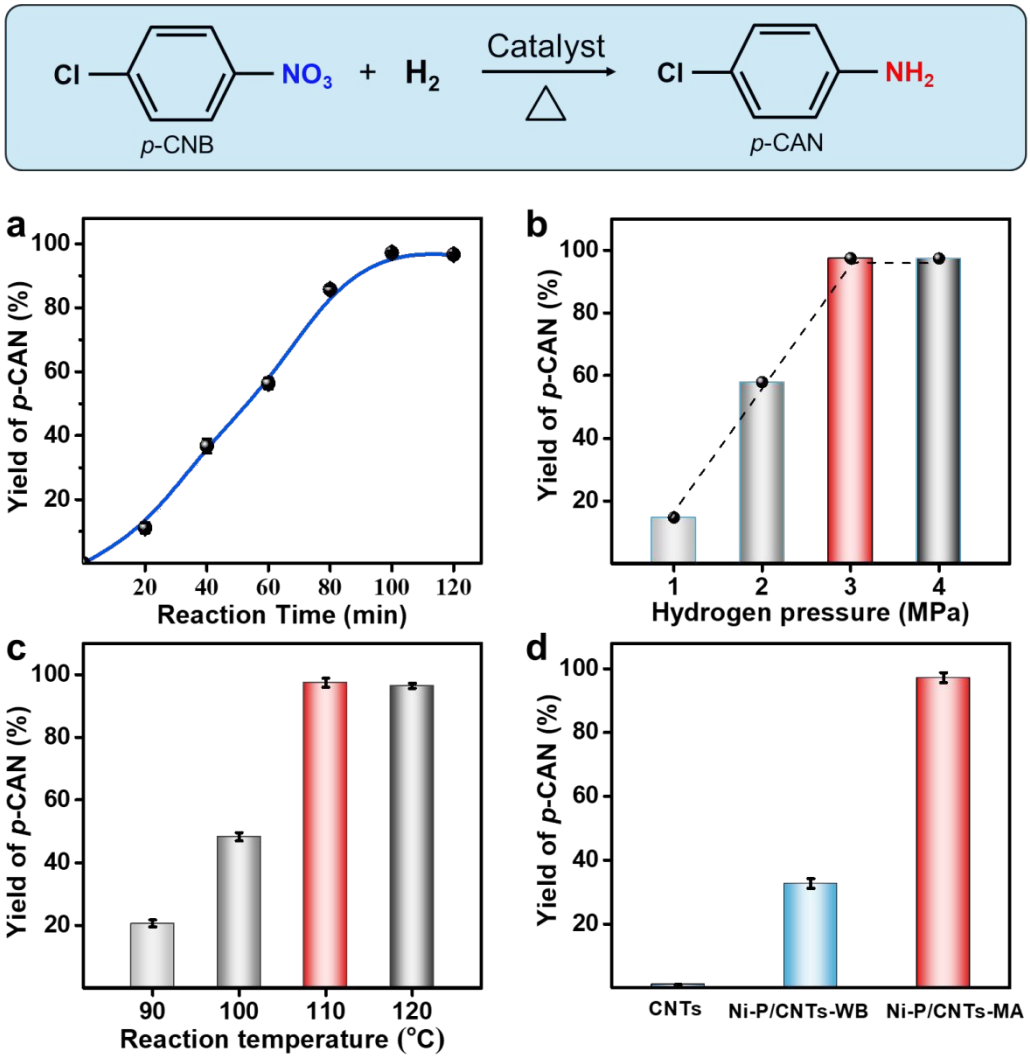

Fig. 3. (a) The hydrogenation activity of *p*-CNB of Ni-P/CNTs-MA with different reaction time at $P(H_2)$ = 3 MPa and T = 110 °C. (b) The activity of Ni-P/CNTs-MA at different hydrogen pressure at T = 110 °C and reaction time = 100 min. (c) The activity of Ni-P/CNTs-MA at different reaction temperatures at $P(H_2)$ = 3 MPa and reaction time = 100 min. (d) The activity of bare CNTs, Ni-P/CNTs-WB and Ni-P/CNTs-MA at conditions of $P(H_2)$ = 3 MPa, T = 110 °C and reaction time = 100 min. Other Reaction conditions: 0.14 mmol Ni, 7.0 mmol *p*-CNB, 20 mL EtOH, stirring rate = 1050 rpm.

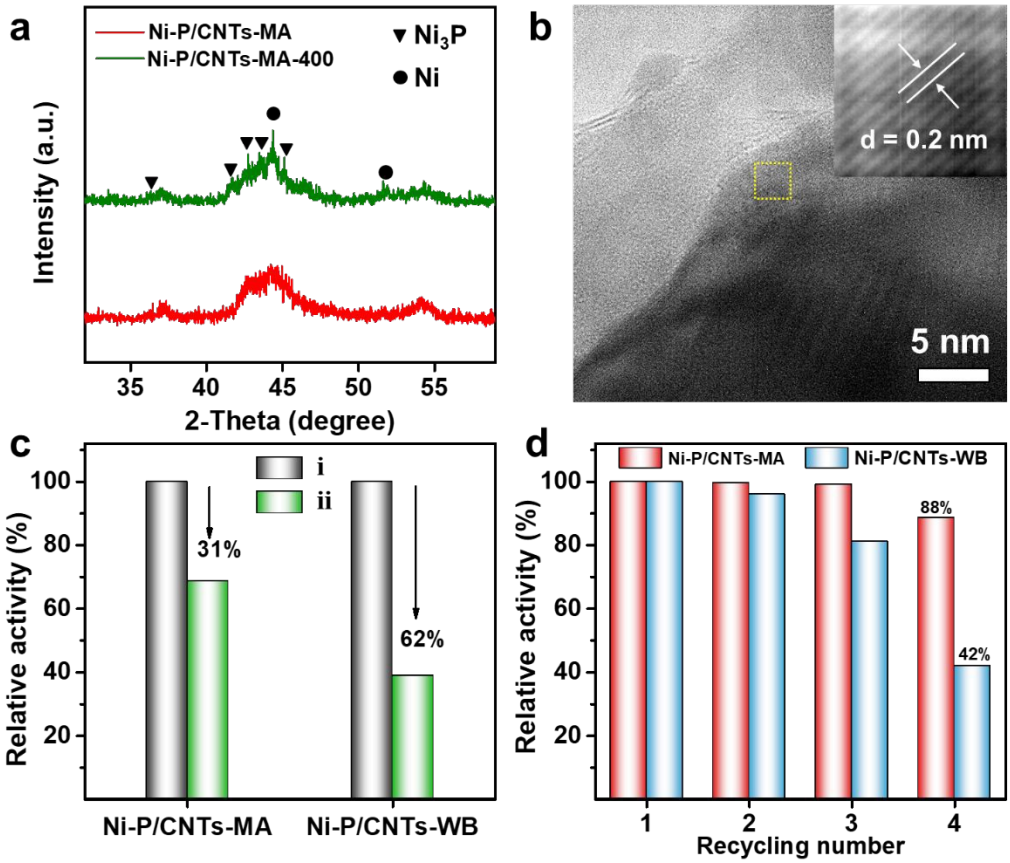

Fig. 4. (a) XRD patterns of fresh Ni-P/CNTs-MA, and Ni-P/CNTs-MA sample thermally treated in N_2 flow at 400 °C for 2 h (Ni-P/CNTs-MA-400). (b) TEM image of Ni-P/CNTs-MA-400. Inset shows an enlarged HRTEM image of selected area in (b). (c) Thermal stability of Ni-P/CNTs-MA and Ni-P/CNTs-WB for *p*-CNB hydrogenation: (i) fresh samples, (ii) samples thermal treated in N_2 flow at 400 °C for 2 h (*i.e.*, Ni-P/CNTs-MA-400 and Ni-P/CNTs-WB-400). (d) Recycling tests of Ni-P/CNTs-MA and Ni-P/CNTs-WB for *p*-CNB hydrogenation.

Table 1. Structural and composition parameters of the catalysts and CNTs.

Sample	Ni wt.%	P wt.%	Molar ratio of Ni-P	Metal dispersion (%)	Metal surface area (m^2/g_{sample})	S_{BET} (m^2/g_{sample})	Pore Volume (cm^3/g)
Ni-P/CNTs-MA	4.16	0.36	$Ni_{88}P_{12}$	21.2	6.2	124.1	0.454
Ni-P/CNTs-WB	4.23	0.28	$Ni_{90}P_{10}$	16.1	4.6	126.9	0.475
CNTs						131.2	0.510

Table 2. Hydrogenation of nitroarenes by Ni-P/CNTs-MA and Ni-P/CNTs-WB catalyst. (Reaction conditions: 0.14 mmol Ni, 7.0 mmol substrate, 20 mL EtOH, T = 110 °C, $p(H_2)$ = 3 MPa, stirring rate = 1,050 rpm.)

Catalyst	Substrate	Product	Reaction time (h)	Conversion (%)	Selectivity (%)
Ni-P/CNTs-MA	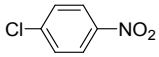	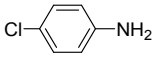	1.7	98.9	98.6
Ni-P/CNTs-WB				33.0	>99
Ni-P/CNTs-MA	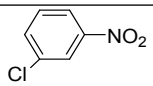	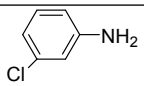	1.5	>99	97.8
Ni-P/CNTs-WB				30.5	>99
Ni-P/CNTs-MA	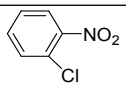	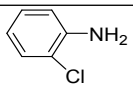	2.0	96.7	>99
Ni-P/CNTs-WB				34.5	>99
Ni-P/CNTs-MA	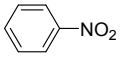	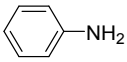	2.5	98.2	>99
Ni-P/CNTs-WB				30.0	>99
Ni-P/CNTs-MA	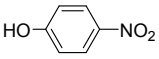	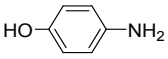	5.5	98.7	>99
Ni-P/CNTs-WB				34.9	>99
Ni-P/CNTs-MA	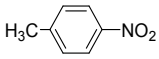	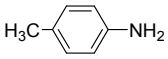	3.5	>99	>99
Ni-P/CNTs-WB				32.6	>99